AJS

Algerian Journal of Sciences
Volume 2 – Issue 1 – PP. 15 – 24

# Galvanostatic growth of zinc oxide nanostructures and their application in photocatalysis

Djamel Selloum[1*], Fatima Zohra Nouasria[2], Sarra Mouffok[3]

[1] Laboratoire Croissance et Caractérisation de Nouveaux Semi-conducteurs, département de chimie, faculté des sceinces, Université Ferhat Abbas Sétif-1, 19000, Algérie

[2]Lab. Dynamic Interactions and Reactivity of Systems, Kasdi Merbah University, Ouargla, 30000, *Algeria*

[3]Centre de Recherche Scientifique et Technique en Analyses Physico-Chimiques (CRAPC), 30000, Ouargla, Algeria

## Abstract

In this study, zinc oxide (ZnO) nanostructures were successfully deposited on indium-doped tin oxide (ITO) using the electrochemical method. The deposition was performed at a constant current density for various deposition times. The potential-time response was recorded and analyzed. X-ray diffraction (XRD) revealed that the ZnO nanostructures had a wurtzite structure with preferential orientation along the (002) axis. The morphology of the samples showed that surface evolution is influenced by deposition time. Additionally, the photocatalytic activity of the ZnO nanostructures was evaluated for the photodegradation of methylene blue, achieving a maximum efficiency of 72.2%, demonstrating the photocatalytic potential of ZnO grown by the galvanostatic method.

**Keywords:** Zinc Oxide, Photocatalysis, Electrochemical Deposition, Current Density, Deposition Time.

**Article History**
Received: 19-10-2024
Accepted: 18-07-2025
Published: 30-09-2025

## 1 Introduction

The advanced technology industry is now focused on developing new materials, particularly miniature materials (nanomaterials) with uniform nanostructural properties, using cost-effective and efficient techniques. Semiconductor nanomaterials represent one of the most diverse classes of nanomaterials. In recent years, there has been growing scientific interest in zinc oxide (ZnO) due to its exceptional properties. ZnO is an intrinsic semiconductor with a wide bandgap of 3.37 eV at room temperature and a high exciton binding energy of 60 meV. It is also recognized for its high transparency, non-toxicity, and thermal and chemical stability [1-3]. These properties have motivated many researchers to explore ZnO for various applications [4-7]. Out of these applications, the photocatalytic application of ZnO has been extensively utilized as a catalyst for water purification [8-10]. Significant effort has been devoted to the fabrication of ZnO nanostructures with various dimensions [11].

* Corresponding author
Email (selloumdjamel@gmail.com)

These nanostructures can be synthesized through physical methods such as physical vapor deposition (PVD) [12], sputtering [13], and molecular beam epitaxy (MBE) [14], as well as chemical methods like chemical vapor deposition (CVD) [15,16], hydrothermal [17,18] sol-gel [19] and electrodeposition [20-22]. Among these techniques, the electrochemical method is the most straightforward, due to its simple working conditions, such as low temperature, cost-effectiveness, environmental friendliness, and suitability for large-scale deposition, which allows for excellent control over the morphology of ZnO structures. This method is typically carried out either in potentiostatic or galvanostatic mode, with the former being more widely studied [22,23]. Additionally, most photocatalytic applications using ZnO as a catalyst have been synthesized via the potentiostatic mode [24,25]

In this study, we will investigate the effect of galvanostatic deposition mode on the photocatalytic application of zinc oxide (ZnO) nanostructures. The ZnO films will be grown at a constant current density and used for the depollution of the aquatic environment, specifically targeting methylene blue (MB) as the organic pollutant. We will vary the deposition time, using three different durations, to observe its impact on the morphological, structural, and optical properties of the ZnO nanostructures.

# 2 Experimental

We used an experimental setup consisting of a classical three-electrode cell. Zinc oxide (ZnO) thin films were electrodeposited onto a glass substrate coated with indium-doped tin oxide (ITO), which has a sheet resistance of 30 Ω /square and served as the working electrode. The active surface area of the electrode was 1 cm2. Prior to deposition, the substrate was cleaned to remove surface impurities by ultrasonic treatment: 10 minutes in acetone, followed by 10 minutes in ethanol, and finally in diluted HNO3, with rinsing in deionized water between each cleaning step. A platinum wire was used as the counter electrode, and a saturated calomel electrode (SCE) was employed as the reference electrode.

To grow ZnO thin films, an aqueous solution containing 5 × 10-3M Zn(NO3)2, which serves as the precursor for both Zn2+ and OH□ ions, and 0.1 M KNO3 as a supporting electrolyte, was prepared. The pH of the solution was adjusted to 5.5, and all solutions were prepared using double-distilled water. Zinc oxide nanostructured films were electrodeposited at a constant current density (J = -0.16 mA/cm2) for three different deposition times (Table 1). The bath temperature was maintained at 70°C. Electrochemical measurements were performed using a potentiostat-galvanostat (PGSTAT204), and the deposition process was conducted without stirring. Additionally, the samples were not subjected to any annealing treatment. We evaluated the photocatalytic efficiency of the ZnO thin films using methylene blue (MB) as the organic pollutant.

Table 1. Electrodeposition parameters used for sample preparation

| **Sample** | **- J (mA.cm$^{-2}$)** | **Deposition time (second)** |
|---|---|---|
| A | 0.16 | 3600 |
| B | 0.16 | 5400 |
| C | 0.16 | 7200 |

# 3 Characterization

The morphology and chemical composition of the prepared films were characterized using scanning electron microscopy (TESCAN, VEGA3-SBH). The structural and crystallographic orientations of the films were analyzed with an X-ray diffractometer (MiniFlex Benchtop) employing monochromatic Cu Kα radiation (λ = 1.54 Å). Optical absorption measurements were performed using a UV-Vis spectrometer (UV-2300).

# 4 Results and discussion

## 4.1 Electrochemical deposition

Figure 1 shows the potentiostatic curves (J = -0.16 mA/cm$^2$) for ZnO deposition at different times and at a fixed temperature of 70°C. A decrease in potential toward more negative values can be observed, which is attributed to the initial stage of ZnO formation (generation of $OH^-$ ions). These ions are produced by the electroreduction of nitrate ions, which chemically react with $Zn_{2+}$ ions to form $Zn(OH)_2$ on the cathode substrate, as reflected by the increase in the potential curve. Finally, ZnO seeds are obtained through the spontaneous dehydration of $Zn(OH)_2$ at temperatures ranging from 60 to 90°C, as shown in the following reaction [26] :

$Zn(NO_3)_2 \longrightarrow Zn^{+2} + NO_3^-$ ……..(1)

$NO_3^- + H_2O + 2e^- \longrightarrow NO_2^- + 2OH^-$ ……...…..(2)

$Zn^{+2} + 2OH^- \longrightarrow Zn(OH)_2$ ……..…..(3)

$Zn(OH)_2 \longrightarrow ZnO + H_2O$ ……...…….(4)

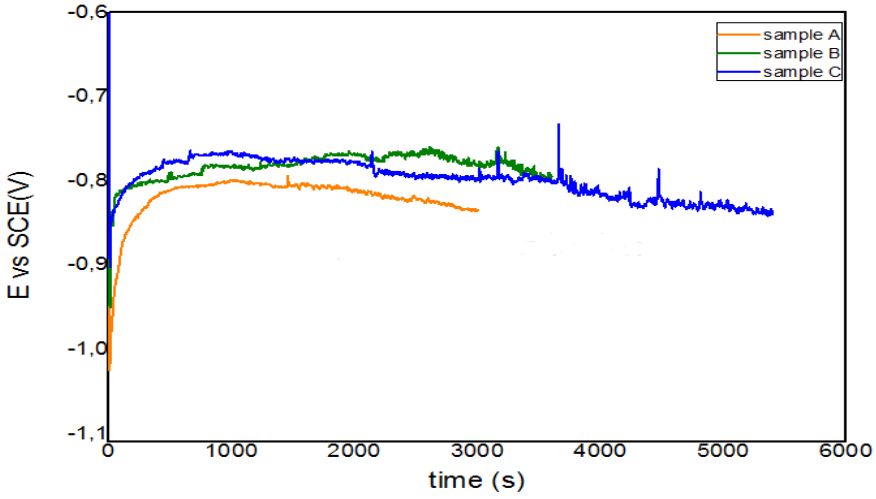



Figure. 1: Chronopotentiograms obtained during deposition of ZnO at different times

(A): 3600(s), (B) :5400(s) , and (C) : 7200(s) from an electrolyte containing $5.10^{-3}$ M $Zn(NO_3)_2$ and 0.1 M $KNO_3$ at 70°C

For all three depositions, an initial significant increase in potential was observed during the first few seconds, followed by a relatively steady decrease until stabilization. Similar behavior was reported by Wadowska et al. [27] when using galvanostatic mode at room temperature.

## 4.2 Structural characterization (XRD)

Figure 2 shows the X-ray diffraction (XRD) patterns of ZnO films deposited at an applied current density of −0.16 mA/cm$^2$ for various deposition times, recorded over a range of 10° to 90° with a scanning step of 0.02°. As the deposition time increases, the samples exhibit similar peak orientations along the (002) c-axis, but with varying intensities due to the continuous growth of ZnO perpendicular to the substrate and the improvement in the films' crystallinity. No peaks corresponding to Zn or other impurities were detected. The narrow and sharp peaks confirm the enhanced crystallinity of the films, and the data indicate the wurtzite structure of ZnO, as referenced by JCPDS card No. 01-080-0075.
Table 2 summarizes the calculated values of crystallite size, dislocation density, and microstrain for the samples. The particle size was calculated by applying the Debye-Scherrer equation [28] to the XRD patterns:

$$D = \frac{K\lambda}{\beta \cos\theta} \quad \text{.....(5)}$$

Where K is the crystallite shape factor, often approximated as 0.9; λ is the X-ray wavelength; β is the full width at half maximum (FWHM) of the X-ray diffraction peak in radians; and θ is the Bragg's angle (in degrees).
The dislocation density (δ) and microstrain (ε) were calculated using equation (6) and (7) respectively [28] :

$$\delta = \frac{1}{D^2} \quad \text{..... (6)}$$

$$\varepsilon = \frac{\beta}{4\tan\theta} \quad \text{.....(7)}$$

Table 2. Value of (FWHM,D,δ, ε) for ZnO samples (A),(B) and (C)

| sapmle | A | B | C |
|---|---|---|---|
| Position peak 2θ(°) | 34.42301 | 34.42572 | 34.45276 |
| FWHM (°) | 0.22306 | 0.21466 | 0.2176 |
| D (nm) | 37.28467839 | 38.74397322 | 38.22329754 |
| $\delta \times 10^{-4}$ (nm$^{-2}$) | 7.1934826 | 6.6618015 | 6.84453105 |
| $\varepsilon \times 10^{-2}$ | 0.03014955 | 0.02901661 | 0.02943858 |

As shown in Table 2, the particle size of ZnO films increased from 37.28 nm to 38.22 nm as the deposition time increased from 3600 to 7200 s. Similarly, the dislocation density (δ) and lattice strain (ε) of the ZnO thin films followed the same trend, decreasing from 7.19 × $10^{-4}$ to 6.84 × $10^{-4}$ nm$^{-2}$ and from

$0.03 \times 10^{-2}$ to $0.02 \times 10^{-2}$, respectively, with increasing deposition time. This reduction in dislocation density and microstrain indicates fewer lattice defects and the formation of higher-quality films.

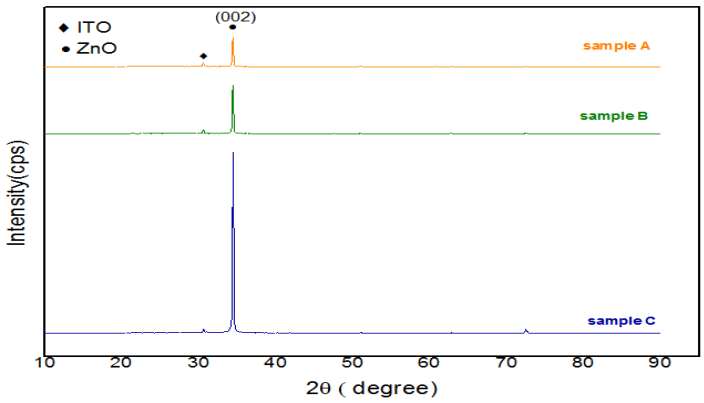



Figure 2: DRX spectra of ZnO layers deposited at different times (A): 3600(s), (B):5400(s), and (C): 7200(s)

## 4.3 Morphological properties

The morphology of the samples (A), (B), and (C) was observed using scanning electron microscopy. Figure 3.A, corresponding to a deposition time of 3600 s, shows small granules scattered across the sample area, with an initial observation of granule coalescence. As the deposition time increased to 5400 s, the surface became more densely covered, and the number of combined granules also increased. At 7200 s, corresponding to sample (C), full surface coverage was observed. Energy dispersive X-ray (EDX) analysis revealed only $Zn^{2+}$ and $O^{2-}$ ions present in the samples, indicating a pure zinc oxide composition.

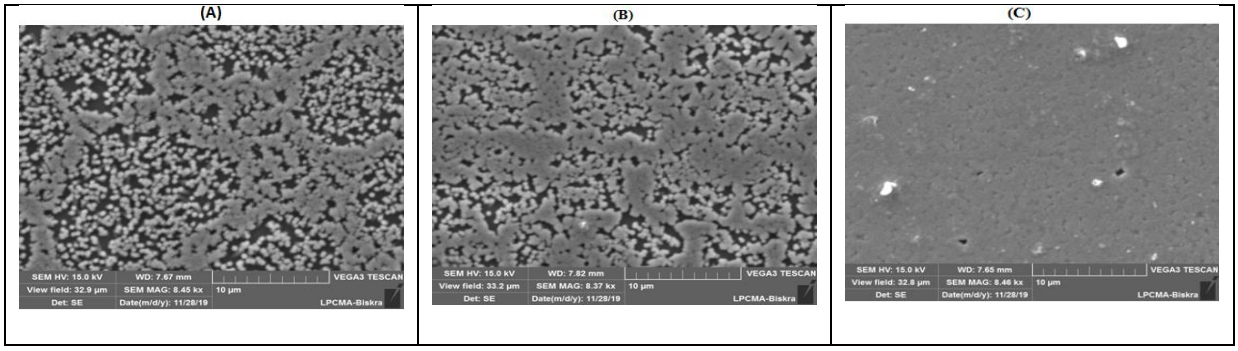



Figure 3: images of scanning electron microscopy for ZnO samples (A),(B) and(C)

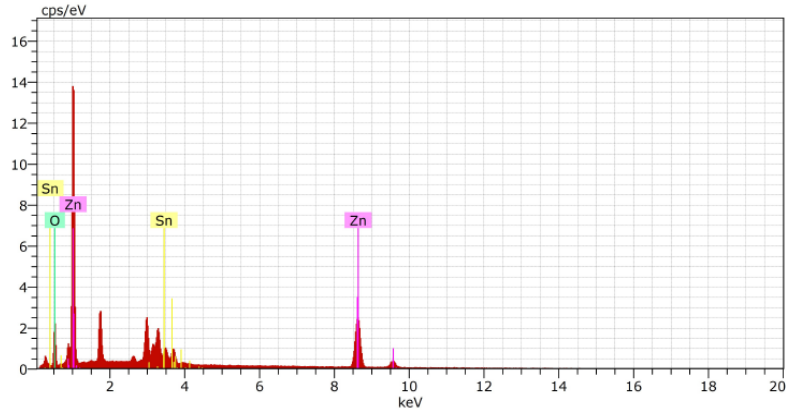



Figure 4: EDX for ZnO thin films: sample (C)

## 4.4 Optical Properties (UV-VIS)

The UV-Vis absorption spectra of the samples were recorded in the wavelength range of 300–800 nm, as shown in Fig. 5. The visible absorption of the thin films decreased with increasing deposition time. Furthermore, a redshift in the absorption edge was observed for ZnO films (B) and (C) compared to ZnO film (A). This shift can be attributed to changes in morphology and particle size. The optical band gap of the samples was estimated using the Tauc formula (Eq. 8):

$$\alpha h\nu = A\,(h\nu - E_g)^n \quad \ldots\ldots\ldots\ldots\ldots\ldots\ldots\ldots\ldots\ldots(8)$$

α is the absorption coefficient, hν is the photon energy, A is a constant, Eg is the energy of the optical band gap, and n is the power factor of the transition mode, which is equal to ½ for direct allowed transitions. By plotting $(\alpha h\nu)^2$ versus hν, we estimated the band gap (Eg) by extrapolating the linear portion of the plot to $(\alpha h\nu)^2 = 0$. The results shown in Fig. 3 were 3.08 eV, 3.27 eV, and 3.34 eV for samples (A), (B), and (C), respectively. This decrease in the ZnO optical band gap is consistent with the corresponding redshift observed in the absorption edge mentioned above.

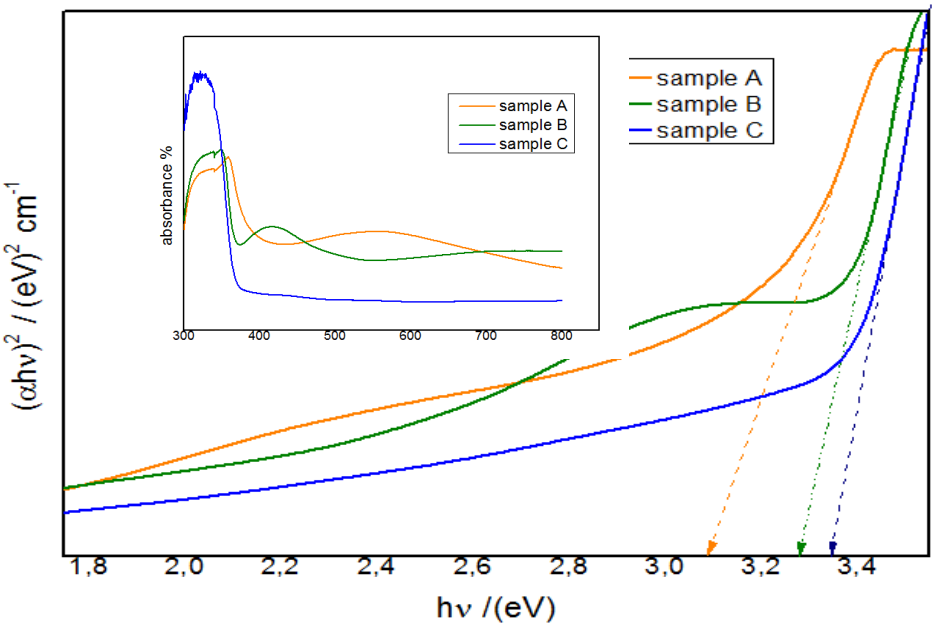



Figure 5: Optical absorption spectra (inset) and bandgap of the prepared ZnO (A: 3600 s), (B: 5400 s) and (C: 7200 s)

## 4.5 Photocatalytic activity

The photocatalytic activity of ZnO thin films was evaluated by studying the photodegradation of methylene blue (MB) as a model pollutant with an initial concentration of 4 ppm. The photocatalytic reactions were conducted under a UV lamp emitting at 365 nm. The progress of the reaction was monitored using a UV-Vis spectrophotometer, with periodic recordings of the absorption spectra to track changes in the concentration of the organic dye over time. The residual dye content was determined using a degradation rate defined as follows (Eq. 9):

$$X = \left(\frac{A_0 - A}{A_0}\right) * 100\% \quad \text{.....(9)}$$

Where $A_0$ and A represent the initial absorbance and the absorbance measured at the maximum wavelength of the dye, respectively. The results are presented in Figures 6 and 7 (a, b), showing that the absorption peak for MB gradually decreases in intensity with increasing exposure time to UV radiation. The degradation rate increased from 19% to 72.2% over an irradiation time of 4 hours. Additionally, the effectiveness of photocatalysis was enhanced by the presence of ZnO nanostructures compared to degradation performed without them, with degradation efficiencies of 72.2% and 49%, respectively, after 240 minutes of UV irradiation. Thus, we conclude that our synthesized films are promising candidates for the degradation of methylene blue.

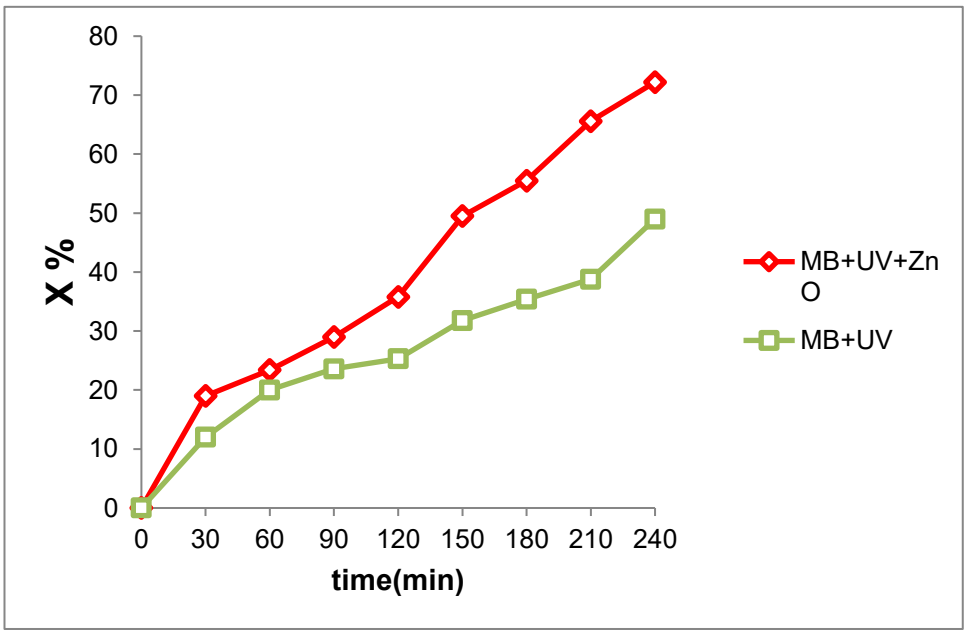



Figure 6: Evolution of degradation rate of MB solution with various irradiation times.

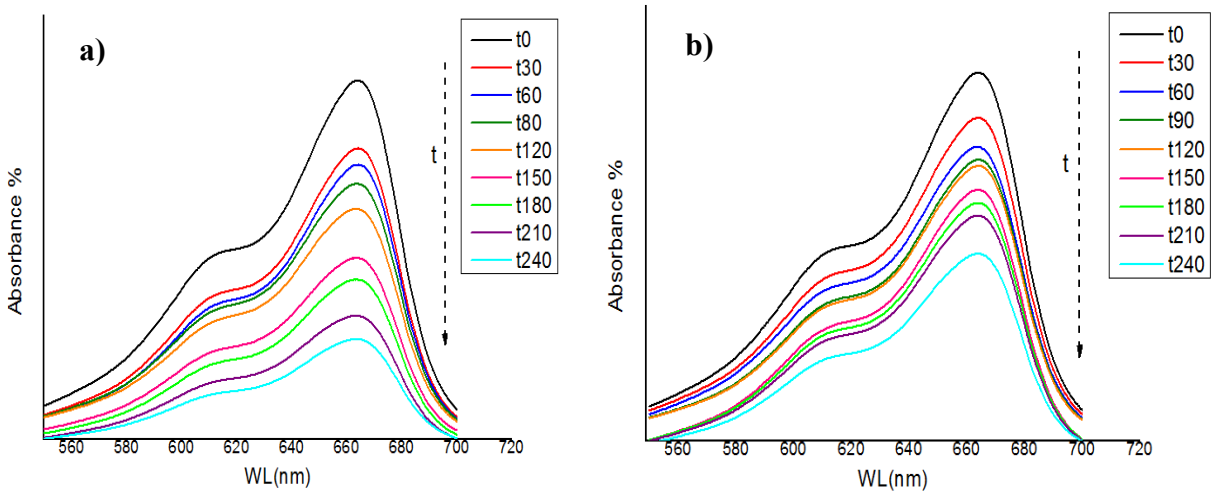



Figure 7: Absorbance spectra of methylene blue versus irradiation time for: left (a) in presence of ZnO and right (b) in the absence of ZnO.

A simplified mechanism for the photocatalytic process of a semiconductor is illustrated in Figure 8, using ZnO nanostructures as the photocatalyst.

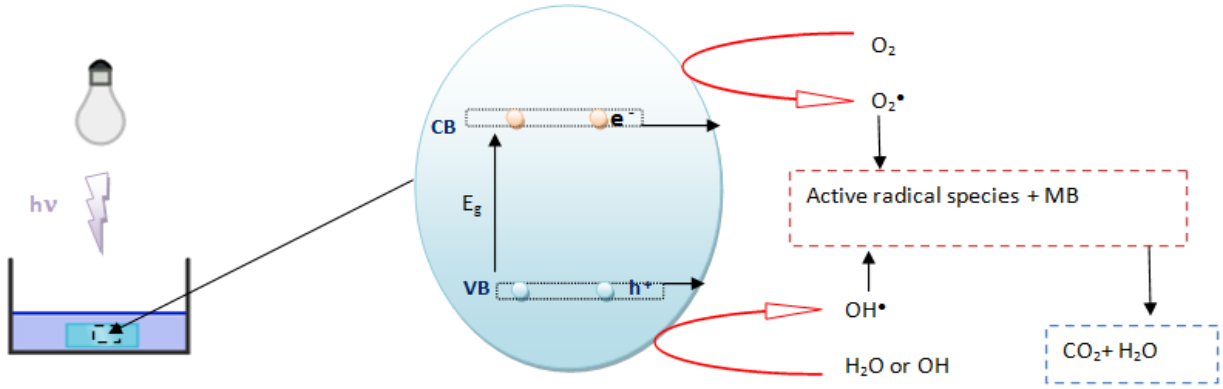



Figure 8: Principle of photocatalysis based on ZnO nanostructures: the electronic process.

# 5 Conclusion

Zinc oxide nanostructures were deposited onto a glass substrate using the electrochemical method. The photocatalytic activities, as well as the structural, morphological, and optical properties of the synthesized films, were investigated. X-ray diffraction confirmed the presence of a polycrystalline ZnO phase with a hexagonal structure. Morphological analysis indicated that varying the deposition time significantly impacts the physical parameters of the grown structures. Zinc oxide nanostructures were found to be effective catalysts for the photodegradation of methylene blue in water under UV irradiation, achieving a high photocatalytic activity of 72.2% over a duration of 4 hours.

# References


[1] Chen, H.M., Chen, C.K., Tseng, M.L., Plasmonic ZnO/Ag embedded plasmonics as collecting layers for photo-generating electrons in solar hydrogen generation photoelectrode, Small, 2013, vol. 9, p. 2926. https://doi.org/10.1002/smll.201202547.

[2] Huang, M.C., Wang, T.H., Cheng, S.H., The structure and photoelectrochemistry of Al, Ti co-doped zinc oxide thin films prepared by sol–gel dip-coating process Nanosci. Nanotechnol. Lett., 2014, vol. 6, p. 210. https://doi.org/10.1166/nnl.2014.1754.

[3] Suliman, A.E., Tang, Y., Xu, L., Preparation of ZnO nanoparticles and nanosheets and their application to dye-sensitized solar cells, Sol. Energy Mater. Sol. Cells., 2007, vol.91, p. 1658. https://doi.org/10.1016/j.solmat.2007.05.014.

[4] Dhamodharan, P., Manoharan, C., Bououdina, M., Al-doped ZnO thin films grown onto ITO substrates as photoanode in dye sensitized solar cell, Sol. Energy., 2007, vol.141, p. 127. https://doi.org/10.1016/j.solener.2016.11.029.

[5] Jeem, M., Zhang, L., Ishioka, J., Tuning Optoelectrical Properties of ZnO Nanorods with Excitonic Defects via Submerged Illumination, Nano Lett., 2017, vol.17, p. 2088. https://doi.org/10.1021/acs.nanolett.7b00324.

[6] Choi, M., Murillo, G., Hwang, S., Mechanical and electrical characterization of PVDF-ZnO hybrid structure for application to nanogenerator, Nano Energy., 2017, vol. 33, p. 462. https://doi.org/10.1016/j.nanoen.2017.01.062.

[7] Al-Hadeethi, Y., Umar, A., Al-Heniti, S.H., 2D Sn-doped ZnO ultrathin nanosheet networks for enhanced acetone gas sensing application, Ceram. Int., 2017, vol.43, p. 2418. https://doi.org/10.1016/j.ceramint.2016.11.031.

[8] Chowdhury, M.I.H., Hossain, M.S., Azad, M.A.S., Photocatalytic degradation of methyl orange under UV using ZnO as catalyst, International Journal of Scientific & Engineering Research, 2018, vol.9, p. 1646. https://doi.org/10.14299/ijser.2018.06.

[9] Adeleke, J.T., Theivasanthi, T., Thiruppathi, M., Photocatalytic degradation of methylene blue by $ZnO/NiFe_2O_4$ nanoparticles, Applied Surface Science, 2018, vol.455, p. 195. https://doi.org/10.1016/j.apsusc.2018.05.184.

[10] Kaur, J., Bansal, S., Singhal, S., Photocatalytic degradation of methyl orange using ZnO nanopowders synthesized via thermal decomposition of oxalate precursor method, Physica B: Condensed Matter, 2013, vol.416, p. 33. https://doi.org/10.1016/j.physb.2013.02.005.

[11] Thangadurai, P., Beura, R., Kumar, J.S., Nanomaterials with Different Morphologies for Photocatalysis, Green Photocatalysts. Environmental Chemistry for a Sustainable World, 2019, vol. 34, p. 47. https://doi.org/10.1007/978-3-030-15608-4_3.

[12] Jouya , M., Taromian, F., Siami, S., Rapid growth of zinc oxide nanobars in presence of electric fieldby physical vapor deposition, J. of Theoretical and Applied Physics, 2018, vol. 11, p. 291. https://doi.org/10.1007/s40094-017-0270-z.

[13] Murkute, P., Ghadi, H., Saha, S., Enhancement in optical characteristics of c-axis-oriented radio frequency–sputtered ZnO thin films through growth ambient and annealing temperature optimization, Mater. Sci. Semicond. Process., 2017, vol.66, p. 1. https://doi.org/10.1016/j.mssp.2017.03.026.

[14] Abdullah, M. M. A., Jamaludin, L., Razak, R. A., p-Type Conductivity Control in ZnO Films Grown by Molecular-Beam Epitaxy, Materials Science Forum, 2016, vol. 75, p. 131. https://doi.org/10.4028/www.scientific.net/MSF.857.131.

[15] Escalante, G., Juárez, H., Fernández, P., Characterization and sensing properties of ZnO film prepared by single source chemical vapor deposition, Adv. Powder Technol., 2017, vol. 28, p. 23. https://doi.org/10.1016/j.apt.2016.07.005.

[16] Fujisawa, H., Kobayashi, C., Nakashima, S., Two-step growth of ZnO nanorods by using MOCVD and control of their diameters and surface densities, J. Korean Phys. Soc., 2013, vol. 62, p. 1164. https://doi.org/10.3938/jkps.62.1164.

[17] Yu, J., Huang, B., Qin, X., Hydrothermal synthesis and characterization of ZnO films with different nanostructures, Appl. Surf. Sci., 2011, vol. 257, p. 5563. https://doi.org/10.1016/j.apsusc.2011.01.039.

[18] Zhang, C., Shao, M., Ning, F., Au nanoparticle sensitized ZnO nanorod@nanoplatelet core-shell arrays for enhanced photoelectrochemical water splitting, Nano Energy., 2015, vol. 12, p. 231. https://doi.org/10.1016/j.nanoen.2014.12.037.

[19] Mahdavi, R., Talesh, S.S.A., The effect of ultrasonic irradiation on the structure, morphology and photocatalytic performance of ZnO nanoparticles by sol-gel method, Ultrason. Sonochem., 2017, vol. 39, p. 504. https://doi.org/10.1016/j.ultsonch.2017.05.012.

[20] Lakhdari, M., Habelhames, F., Nessark, B., Effects of pulsed electrodeposition parameters on the properties of zinc oxide thin films to improve the photoelectrochemical and photoelectrodegradation efficiency, Eur. Phys. J. Appl. Phys., 2018, vol.84, p. 1. https://doi.org/10.1051/epjap/2018180227.

[21] Salazar, R., Saidi, B., Delamoreanu, A., Electrochemical growth of hexagonally arranged ZnO nanowall structures on ZnO substrates. Influence of surface polarity, J. of Electro. Chem., 2019, vol.850, p. 1. https://doi.org/10.1016/j.jelechem.2019.113397.

[22] Burgos, A., Schrebler, R., Cáceres, G., 'Electrodeposition of ZnO Nanorods as Electron Transport Layer in a Mixed Halide Perovskite Solar Cell, Int. J. Electrochem. Sci., 2018, vol. 13, p. 6577. https://doi.org/10.20964/2018.07.25.

[23] Rahal, H., Kihal, R., Affoune, A.M., Electrodeposition and characterization of ZnO thin films using sodium thiosulfate as an additive for photovoltaic solar cells, Journal of Semiconductors, 2017, vol. 38, p. 1. https://doi.org/10.1088/1674-4926/38/5/053002.

[24] Zhang, F., Zhang, W., luo, X., Electrodeposition of ZnOFilm WithEnhanced Photocatalytic Activity Towards Methylene Blue Degradation, Int. J. Electrochem. Sci., 2017, vol.12, p. 3756. https://doi.org/10.20964/2017.05.62.

[25] Taha, S.A., Elnaiem, A.M.A., Mohamed, M., Structural study and photocatalytic performance of ZnO thin films prepared by electrochemical deposition, Desalination and water treatment, 2017, vol. 100, p. 160. https://doi.org/10.5004/dwt.2017.21752.

[26] Chettah, H., Abdi, D., Effect of the electrochemical technique on nanocrystalline ZnO electrodeposition, its structural, morphological and photoelectrochemical properties, Thin Solid Films, 2013, vol. 537, p. 119. https://doi.org/10.1016/j.tsf.2013.04.024.

[27] Wadowska, M., Frade, T., Siopa, D., ZnO nanostructured films electrodeposited at room temperature, ECS Electrochemestry letters, 2013, vol.2, p. D40. https://doi.org/10.1149/2.009307eel.

[28] Salman, O. N., Dawood, M. O., Ali, A. K., Low Cot Synthesis of ZnO nano thin film by electrochimical deposition, Digest Journal of Nanomaterials and Biostructures, 2017, vol. 12, p. 719.